AIAA-98-0602

Inverse Design Method for Wings of Supersonic Transport

Shinkyu Jeong†
Tohoku University, 980-77, Sendai, Japan
Ph:81-22-217-6981, Fax:81-22-217-6979
E-mail:jeong@ad.mech.tohoku.ac.jp

Kisa Matsushima‡
Fujitsu Limited,
Chiba 261, Japan

Toshiyuki Iwamiya†
National Aerospace Laboratory, Chofu, Tokyo 182, Japan

Shigeru Obayashi* and Kazuhiro Nakahashi**
Tohoku University, 980-77, Sendai, Japan

Abstract

A practical inverse design method for supersonic airfoils/wings has been developed. The method is based on Takanashi's iterative "residual-correction" concept. A geometry that materializes a specified pressure distribution is sought by solving an integrodifferential form of the linearized small perturbation (LSP) equation. The integration is limited to the Mach forecone from the point of interest. Several design results are presented.

Nomenclature

ϕ	perturbation velocity potential
C_p	pressure coefficient
ΔC_p	$C_p^{target} - C_p^{computed}$
$f(x, y)$	wing surface coordinate
M_∞	freestream Mach number
ψ	kernel function, Eq. (18)
$\Delta \cdot$	perturbed quantities, $\Delta\phi, \Delta Cp$, etc.
γ	ratio of specific heats
Re	Reynolds number based on root chord length
α	angle of attack

Introduction

With a recent trend of the world wide growth of air transportation, development of a next generation supersonic transport (SST) is under consideration in the Unite States, Europe, and Japan. Although Concorde, the sole existing SST, is a great technological achievement, it was not able to achieve economic success. One of its shortcomings is a low L/D performance. Its poor L/D has to be compensated by high fuel burn, which increases the operating cost. To guarantee economic success of the next generation SST, a higher L/D ratio is indispensable. To achieve this goal, a new design technique for supersonic wings is necessary.

There are several design methods[1,2,3] used for supersonic wings. Most of these methods consider only warp optimization by using the linearized method, however, it is also important to consider wing thickness control to obtain a wing of high performance. Especially, the thickness control plays an important role, such as, for prevention of the leading-edge separation and for laminar flow control.

To optimize both the warp and thickness of a wing simultaneously, Kamiya, et al.[4] suggested an inverse design method using the Prandtl-Meyer function and the linearized theory. However, this method is limited

---

† Graduate Student, Dept. of Aeronautics & Space Engineering

‡ Research Scientist, Supercomputer Systems Engineering Division, Member AIAA

† Head of Applied Math. Lab., Computer Science Division

*Associate Professor, Dept. of Aeronautics & Space Engineering, Senior Member AIAA

**Professor, Dept. of Aeronautics & Space Engineering, Associate Fellow AIAA

to two-dimensional design problems. When this method is applied to a three-dimensional problem, convergence to a target pressure distribution becomes worse because it cannot account for the three-dimensional effect.

In this study, a three-dimensional supersonic wing design method which can design both the warp and thickness at the same time, is developed. The present method is extended from Takanashi's inverse design method[5] used for the transonic wing design. Takanashi solved the inverse problem by using the integral form of the transonic small disturbance equation with "residual-correction" concept. This paper will discuss the mathematical formulation of the present method, followed by several numerical results. These results will confirm the validity of this method.

Design Procedure

The inverse problem for the aerodynamic shape design is to find a geometry that materializes a specified surface pressure distribution. The 'residual-correction' procedure of finding the corresponding geometry can be described as follows. First, a target pressure distribution and an initial wing geometry is selected. The flow analysis is then performed for the initial wing geometry to obtain the surface pressure distribution. The present inverse design method is decoupled from the flow analysis, so the any type of analysis, even an experiment, can be used for the flow analysis. In this paper, the Euler/Navier-Stokes code is used. From the computed and target pressure distributions, the pressure difference is calculated. Using this pressure difference as a boundary condition, the geometry correction is obtained by solving the integrodifferential linearized small perturbation (LSP) equation. By modifying the initial geometry with the geometry correction, a new geometry is produced. This process will be iterated until ΔCp becomes sufficiently small. Figure 1 shows the flowchart of the present inverse design procedure.

Integral Formulation of Inverse Method

In a supersonic flow, the small perturbation potential equation can be expressed in the linearized form as

$$(M_\infty^2-1)\,\bar{\phi}_{\bar{x}\bar{x}}-\bar{\phi}_{\bar{y}\bar{y}}-\bar{\phi}_{\bar{z}\bar{z}}=0 \tag{1}$$

and pressure coefficients on wing surfaces and the tangency conditions can be written as

$$C_{p\pm}(\bar{x},\bar{y})=-2\,\bar{\phi}_{\bar{x}}(\bar{x},\bar{y},\pm 0) \tag{2}$$

$$\frac{\partial\,\bar{f}_{\pm}(\bar{x},\bar{y})}{\partial\bar{x}}=\bar{\phi}_{\bar{z}}(\bar{x},\bar{y},\pm 0) \tag{3}$$

where the subscripts '$\pm$' denote the upper and lower surfaces of the wing. For brevity, the Prandtl-Glauert transformation is used in the above equations as

$$x=\bar{x},\ y=\bar{y},\ z=\bar{z},\ \phi(x,y,z)=\frac{1}{\beta^2}\bar{\phi}(\bar{x},\bar{y},\bar{z}),$$

$$f_{\pm}(x,y)=\frac{1}{\beta^3}\bar{f}_{\pm}(\bar{x},\bar{y}) \tag{4}$$

where $\beta=\sqrt{M_\infty^2-1}$.

The transformed equations are written as

$$\phi_{xx}-\phi_{yy}-\phi_{zz}=0 \tag{5}$$

$$C_{p\pm}\left(x,\frac{y}{\beta}\right)=-2\beta^2\phi_x(x,y,\pm 0) \tag{6}$$

$$\frac{\partial f_{\pm}(x,y)}{\partial x}=\beta^3\phi_z(x,y,\pm 0) \tag{7}$$

Suppose the solution of Eq. (5), $\phi(x,y,z)$, for the initial geometry $f(x,y)$ is given and the perturbation, $\Delta\phi(x,y,z)$, is occurred to this known flow, Eqs. (5)-(7) become

$$(\phi_{xx}+\Delta\phi_{xx})-(\phi_{yy}+\Delta\phi_{yy})-(\phi_{zz}+\Delta\phi_{zz})=0 \tag{8}$$

$$C_{p\pm}\left(x,\frac{y}{\beta}\right)+\Delta C_{p\pm}\left(x,\frac{y}{\beta}\right) \tag{9}$$

$$=-2\beta^2[\phi_x(x,y,\pm 0)+\Delta\phi_x(x,y,\pm 0)]$$

$$\frac{\partial f_{\pm}(x,y)}{\partial x}+\frac{\partial\Delta f_{\pm}(x,y)}{\partial x} \tag{10}$$

$$=\beta^3[\phi_z(x,y,\pm 0)+\Delta\phi_z(x,y,\pm 0)]$$

By subtracting Eqs. (5)-(7) from Eqs. (8)-(10), the perturbation equations are obtained as follows.

$$\Delta\phi_{xx}-\Delta\phi_{yy}-\Delta\phi_{zz}=0 \tag{11}$$

$$\Delta C_{p\pm}\left(x,\frac{y}{\beta^2}\right)=-2\beta^2\Delta\phi_x(x,y,\pm 0) \tag{12}$$

$$\frac{\partial\Delta f(x,y)}{\partial x}=\beta^3\Delta\phi_z(x,y,\pm 0) \tag{13}$$

The solution of Eq. (11), $\Delta\phi$, can be derived by means of Green's theorem[6,7] :

$$\Delta\phi(x,y,z) \tag{14}$$

$$=-\frac{1}{2\pi}\frac{\partial}{\partial x}\int\int_{\tau_1}[(\Delta\phi_\xi(\xi,\eta,+0)-\Delta\phi_\xi(\xi,\eta,-0))$$

$$\times\phi(x,y,z;\xi,\eta,0)]d\xi d\eta$$

$$+\frac{1}{2\pi}\frac{\partial}{\partial x}\int\int_{\tau_1}[(\Delta\phi(\xi,\eta+0)-\Delta\phi(\xi,\eta,-0))$$

$$\times\phi_\xi(x,y,z;\xi,\eta,0)]d\xi d\eta$$

where

$$\phi(x,y,z;\xi,\eta,\zeta)=\cosh^{-1}\frac{x-\xi}{\sqrt{(y-\eta)^2+(z-\zeta)^2}} \tag{15}$$

The integral surface τ_1 is the part of $z=0$ plane contained within the Mach forecone from the point (x,y,z), that is, the area bounded by the line $\xi=-\infty$ and the hyperbola;

$$(x-\xi)^2-(y-\eta)^2-(z-\zeta)^2=0 \tag{16}$$

Namely, the integral surface τ_1 is inside of the Mach forecone on the planform. The integral surface τ_1 on the triangular planform is shown in Fig 2.

To utilize the pressure distribution as a boundary condition, Eq. (14) is differentiated with respect to x and by adding the resulting $\Delta\phi_x(x,y,z)$ at z=+0 and z=-0, we obtain

$$\Delta u_s(x,y)=-\Delta w_s(x,y) \tag{17}$$

$$+\frac{1}{\pi}\int\int_{\tau_1}\frac{(x-\xi)\Delta w_s(\xi,\eta)}{\sqrt{(x-\xi)^2-(y-\eta)^2}^3}d\xi d\eta$$

$$\Delta u_s(x,y)=\Delta\phi_x(x,y,+0)+\Delta\phi_x(x,y,-0) \tag{18}$$

$$\Delta w_s(x,y)=\Delta\phi_z(x,y,+0)-\Delta\phi_z(x,y,-0) \tag{19}$$

Similarly, differentiating both sides of Eq. (14) with respect to z and adding the resulting $\Delta\phi_z(x,y,z)$ at $z=+0$ and $z=-0$, we obtain

$$\Delta w_a(x,y)=-\Delta u_a(x,y) \tag{20}$$

$$+\frac{1}{\pi}\int\int_{\tau_1}\frac{(x-\xi)\Delta u_a(x,y)}{(y-\eta)^2\sqrt{(x-\xi)^2-(y-\eta)^2}}d\xi d\eta$$

$$\Delta u_a(x,y)=\Delta\phi_x(x,y,+0)-\Delta\phi_x(x,y,-0) \tag{21}$$

$$\Delta w_a(x,y)=\Delta\phi_z(x,y,+0)+\Delta\phi_z(x,y,-0) \tag{22}$$

By solving Eqs. (17) and (20) with the boundary conditions Δu_s and Δu_a, the geometry terms Δw_s and Δw_a can be obtained. As defined in Eqs. (19) and (22), $\Delta w_s(x,y)$ and $\Delta w_a(x,y)$ represent the derivatives of thickness and camber corrections, respectively.

The integrated value for the thickness correction , however, doesn't have to satisfy the closure condition at the trailing edge. In this paper, Δw_s are modified so as to satisfy the closure condition. Modifications are performed according to the following equation:

$$\Delta w_s^{\mathrm{mod}}(x,y) \tag{23}$$

$$=\Delta w_s(x,y)-\frac{\int_{L.E}^{T.E}\Delta w_s(\xi,y)\,d\xi}{\overline{dx}}\times\frac{dx}{l}$$

where l is local chord length and $\overline{dx}$ is chord length divided by number of panels at each spanwise location.

The geometry correction can be computed by performing the numerical integration in the x-direction.

$$\Delta f_\pm(x,y) \tag{24}$$

$$=\frac{1}{2}\int_{L.E}^{x}\Delta w_a(\xi,y)d\xi\pm\frac{1}{2}\int_{L.E}^{x}\Delta w_s^{\mathrm{mod}}(\xi,y)\,d\xi$$

This equation may be contrasted with the camber design of Ref. 8.

Since Eqs. (17) and (20) are based on LSP equation, they become invalid where the vorticity is generated. Such regions are typically around the root and tip of the wing. At the wing root, the bilateral symmetry is usually assumed for the flow analysis, but $\frac{\partial p}{\partial y}\neq 0$ when the straight isobar pattern is enforced for prescribing a pressure distribution for a swept wing. This breaks the irrotational flow assumption at the wing root. At the wing tip, on the other hand, the flow is naturally rotational due to the wing tip vortex. Therefore, the Eqs. (17) and (20) should be replaced with lower order approximations in those regions.

$$\Delta u_s(x,y)=-\Delta w_s(x,y) \tag{25}$$

$$\Delta w_a(x,y)=-\Delta u_a(x,y) \tag{26}$$

These equations are now the supersonic linearized pressure coefficient equations.

Results

To confirm the validity of the present formulation of the supersonic inverse method, two- and three-dimensional design results are presented.

Airfoil Design Problem

As a flow analysis code, a Navier-Stokes solver[9] is used. This solver adopted a TVD upwind scheme for the spatial discretization of the convective terms and the LU-SGS method for the time integration. Turbulence effects was evaluated by using the Baldwin-Lomax model.

The computational grid is generated by an algebraic grid generation code. The two-dimensional C-type grid contains 191 cells in the streamwise direction and 91 cells in the normal direction.

Case 1: Reconstruction of a Known Airfoil

The pressure distribution of NACA-1204 airfoil at a flow condition of M_∞=2.0, α=2° and Re=1.45×10^7 is obtained by using the Navier-Stokes solver and designated as the target pressure distribution. As the initial geometry, NACA-0003 airfoil is used. Actually, in the two dimensional inverse design, there is no need to performed the integration expressed in Eqs. (18) and (23) along the spanwise direction but in this paper to validate the mathematical formulation of the supersonic inverse method prescribed above, the 'infinite wing' concept is adopted. Thus, the integrations in Eqs. (18) and (23) are performed on the rectangular planform shown in Fig. 3. 50 panels used for both streamwise and spanwise directions.

Figure 4 shows the design result of this case. Both the geometry and pressure distribution are converged to those of NACA-1204 airfoil after 4 iterations.

Case 2: Changing Angle of Attack

The pressure distribution of NACA-66003 airfoil at the same flow condition as Case 1 is obtained by the Navier-Stokes analysis and designated as the target pressure distribution. In this case, the flow condition is changed to α=0.

The design result is shown in Fig. 5. The designed airfoil is inclined in 2 degrees and its pressure distribution is coincided with that of NACA-66003 airfoil in a flow at M_∞=2.0, α=2° and Re = 1.45×10^7.

Wing Design Problem

The Euler code is used for the three-dimensional flow analysis for a wing. The spatial discretization and time integral method are the same as used in the two-dimensional problem. For a computational grid, the C-H topology is used, applying the two-dimensional grid generation at each spanwise section. The grid consists of $191\times84\times33$ points in the streamwise, spanwise and normal directions, respectively.

The planform used in this three-dimensional wing design problem is shown in Fig. 6. This planform is the so called 0-th baseline configuration of the NAL(National Aerospace Laboratory) SST program. The leading-edge sweep angle is about 70° and the leading- and trailing-edge kinks are located at 43.96 % and 40% spanwise sections, respectively. For inverse design, there are 50 panels in streamwise direction and 67 panels in spanwise direction.

The target pressure distribution is obtained from the untwisted wing based on NACA-1204 airfoil in an inviscid flow at M_∞ = 2.0 and α = 2° . The initial wing is obtained from NACA-0003 airfoil.

Figure 7 shows comparison of surface pressure distributions at six spanwise sections among the target, initial, and designed wings after 6 iterations. Except at the 90% section, pressure distributions of the designed wing coincide with those of the target wing. Discrepancies near the tip is attributed to the invalidity of the irrotational assumption of the original LSP equation there.

To improve the overall convergence, the integrodifferential equation is replaced with the supersonic linearized pressure coefficient equation near the root and tip sections where the original LST equation does not hold.

The corresponding design results are shown in Fig. 8. The designed and target pressures coincide with each other from the root to the tip better. To check the convergence, residual pressure differences ($\overline{\Delta Cp}$) averaged at each spanwise section are plotted in Fig 9. As shown in the figure, the integral equation derived here gives the best convergence in the midspan from 30% to 70% section. On the other hand, near the root and tip, it gives the worst convergence due to the irrelevant physics. The lower order correction based on the supersonic linearized pressure coefficient equation is shown to give the better convergence there. Thus, by switching the both equations, the overall convergence is greatly improved.

Conclusion & Future Works

A new inverse design method for wings of SST has been developed. Takanashi's transonic inverse method is extended to the supersonic wing design. By solving the integrodifferential equation iteratively, corresponding geometry which materializes a specified pressure distribution can be found. In case of three-dimensional problems, the present method is revised by using the supersonic linearized pressure coefficient equation near the wing root and tip where the irrotational flow assumption does not stand. The two- and three-dimensional design results confirmed the validity of this method.

To use this design method effectively, the target pressure distribution must be selected carefully. The design objectives should be translated into the pressure distribution. The determination of an optimal target pressure distribution[10] will be studied in future for the supersonic cases.

References

1. Carlson, H. W. and Miller, D. S., "Numerical Methods for the Design and Analysis of Wings at Supersonic Speed," NASA TN D-7713, 1974.
2. Yoshida, K. and Hayama, K., "Experimental and Numerical Study of Aerodynamic Characteristics for Second generation SST," SAE paper 91-2056, 1991.
3. K. B. Walkley, and G. E. Smith, "Application of a Full Potential Method to Supersonic Aircraft Design and Analysis," *Journal of Aircraft*, Vol. 26, No. 1, pp.6-12, Jan., 1989.
4. Kamiya, N., Tamaki, H., Hirose, N., and Ishida Y., "On an Inverse Problem for a Supersonic Airfoils Based on Navier-Stokes Approximation," Proc. of 14th the NAL Symposium on Aircraft Computational Aerodynamic, 1997 (in Japanese).
5. Takanashi, S., "Iterative Three-Dimensional Transonic Wing Design Using Integral Equations, " *Journal of Aircraft*, Vol. 22, No. 8, pp.655-660, Aug. 1985.
6. Heaslet, M. A., Lomax, H., and Jones, A. L., "Volterra's Solution of the Wave Equation as Applied to Three-Dimensional Supersonic Airfoil Problem," NACA Rep. 899, 1947. (Formerly NACA TN 1412.)
7. Lomax, H., Heaslet, M. A. and Franklyn, B. Fuller, "Integrals and Integral Equation in Linearized Wing Theory," NACA Rep. 1054, 1951.
8. Carlson, H. W. and Middleton, W. D., "A Numerical Method for Design of Camber Surfaces of Supersonic Wings with Arbitrary Planforms," NASA TN-2341, 1964.
9. Obayashi, S. and Guruswamy, G. P., "Navier-Stokes Computations for Oscillating Control Surface, " *Journal of Aircraft*, Vol. 31, No. 3, pp.631-636, May-June, 1994.
10. Obayashi, S., Jeong, S. and Matsuo, Y., "New Blunt Trailing-Edge Airfoil Designed by Inverse Optimization Method," *Journal of Aircraft*, Vol. 34, No. 2, pp.255-257, March-April, 1997.

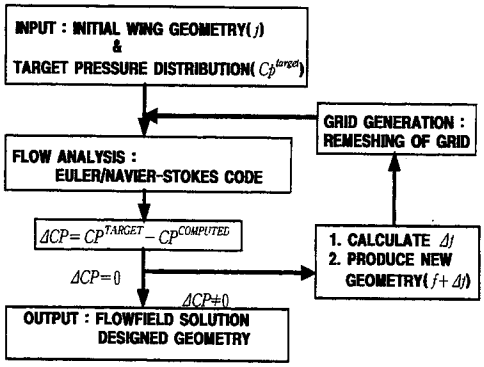

Figure 1. Flowchart of inverse design procedure

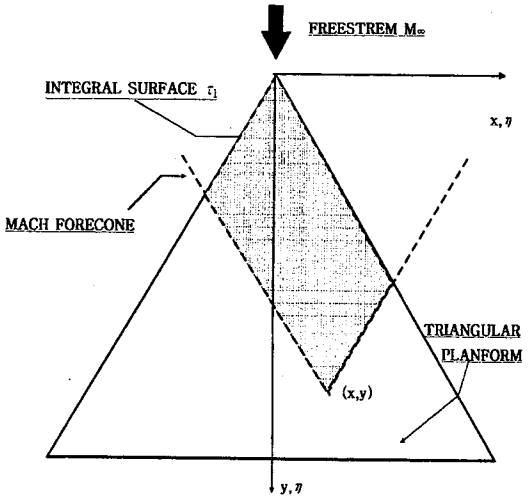

Figure 2. Integral surface on the triangular planform

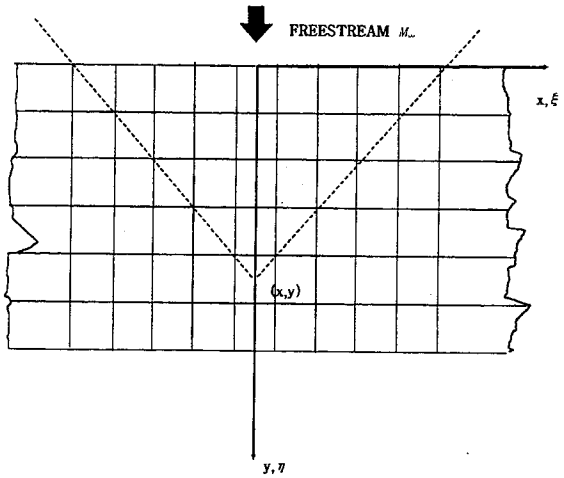

Figure 3. Integral surface on rectangular planform

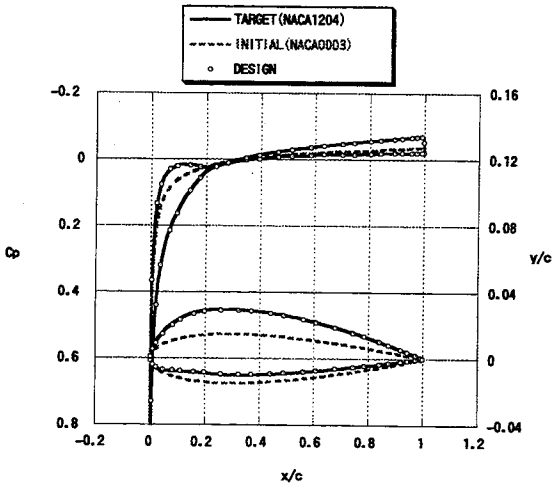

Figure 4. Comparison of the two-dimensional inverse design results

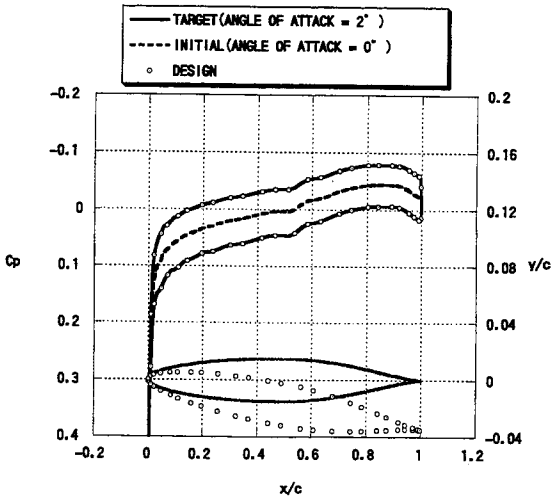

Figure 5. Comparison of the two-dimensional inverse design results

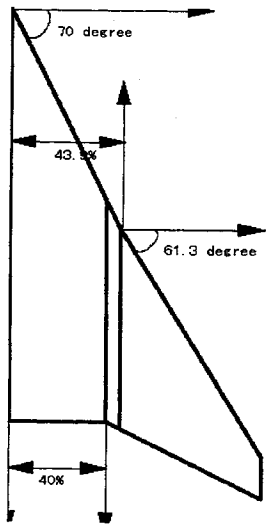

Figure 6. Wing planform

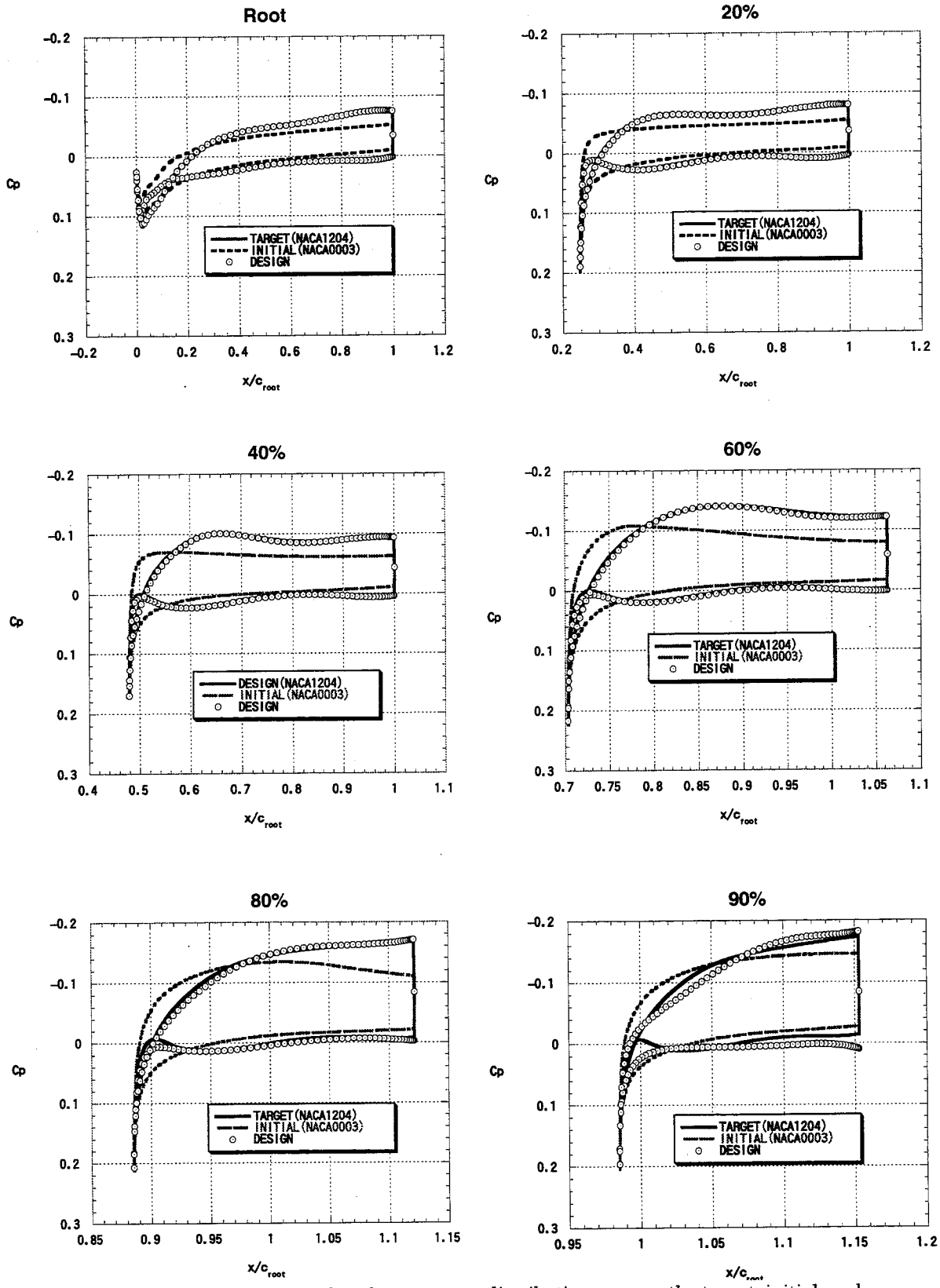

Figure 7. Comparison of surface pressure distributions among the target, initial, and designed wings obtained from the integral equation only.

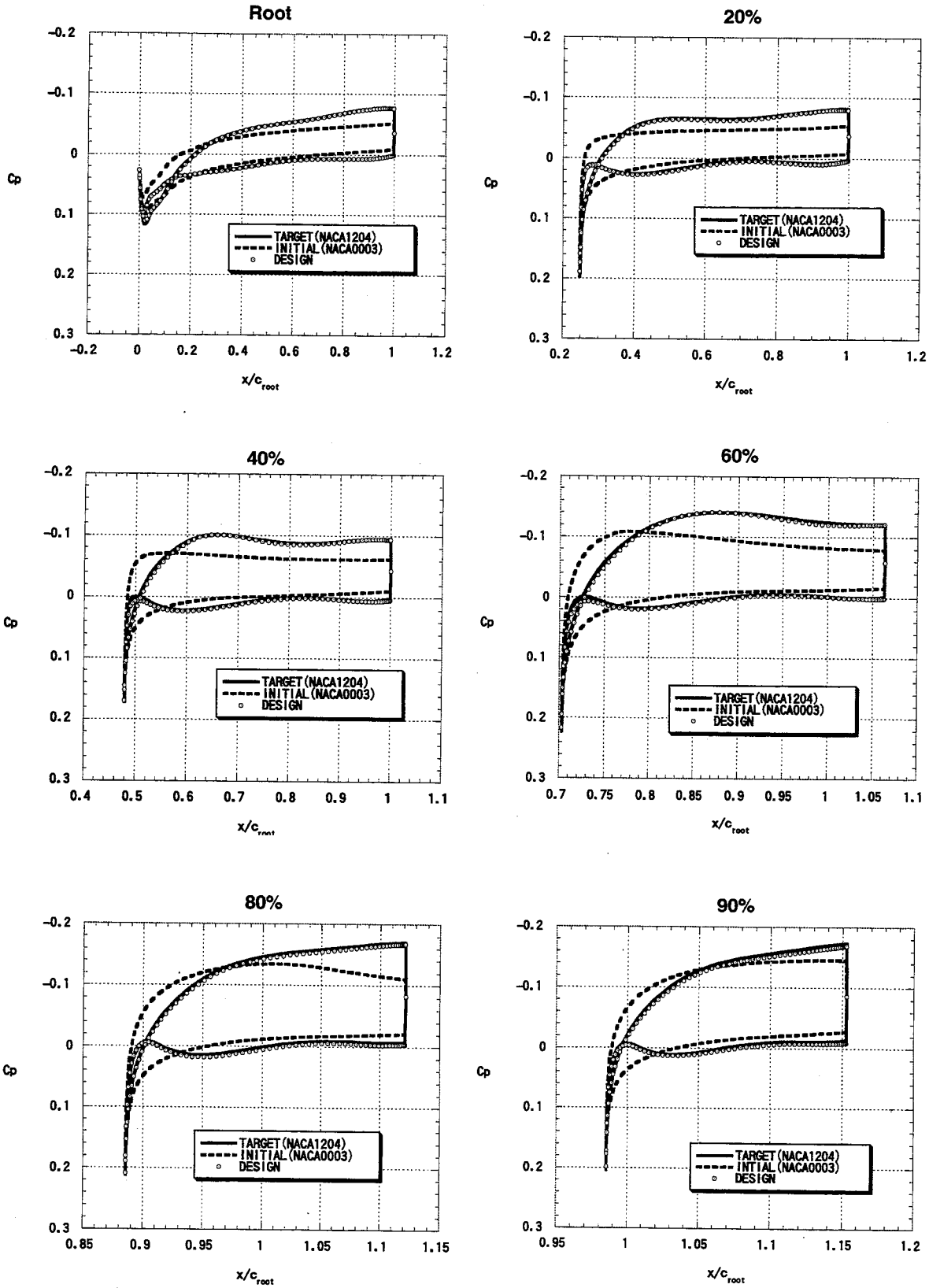

Figure 8. Comparison of surface pressure distributions among the target, initial, and designed wings obtained from the present modified method.

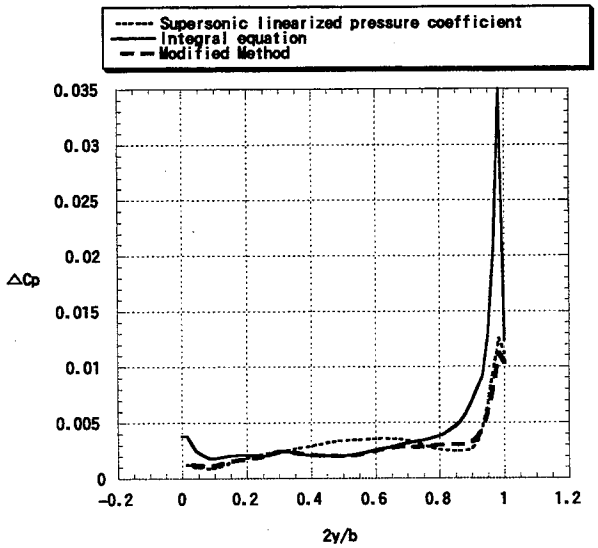

Figure 9. Comparison of spanwise residual pressure difference